PCCP

Accepted Manuscript

ROYAL SOCIETY OF CHEMISTRY

www.rsc.org/pccp

Journal Name

RSCPublishing

ARTICLE

Lithium storage in disordered graphitic materials: a semi-quantitative study of the relationship between structure disordering and capacity

Cite this: DOI: 10.1039/x0xx00000x

Received 00th January 2012,
Accepted 00th January 2012

DOI: 10.1039/x0xx00000x

www.rsc.org/

Tan Xing[a], Thrinathreddy Ramireddy[a], Lu Hua Li[a], Daniel Gunzelmann[a], Hong Zeng[b], Qi Wen[b], Shaoxiong Zhou,[b] and Ying Chen*[a]

[a] Institute for Frontier Materials, Deakin University, Waurn Ponds, VIC 3216, Australia.
[b] China-Australia Joint Research Centre in Energy Nanomaterials, Advance Technology & Materials Co., Ltd, China Iron & Steel Research Institute Group, Beijing 100081, P.R.China

Corresponding author: Ying Chen, 75 Pigdons Road, GTP, Waurn Ponds, VIC3216, Australia
Ph 61 3 52273243, e-mail: ian.chen@deakin.edu.au

Abstract

The application of graphitic anode is restricted by its low theoretical specific capacity of 372 mAh/g. Higher capacity can be achieved in the graphite anode by modifying its structure, but the detailed storage mechanism is still not clear. In this work, the mechanism of the lithium storage in disordered graphitic structure has been systematically studied. It is found the enhanced capacity of distorted graphitic structure does not come from lithium-intercalation, but through a capacitive process which depends on disordering degree and porous structure.

Keywords: graphite, Li-ion battery, ball milling, anode

Introduction

The lithium ion battery has become a very popular power source nowadays. Its performance, however, hinders its practicality in high-power and/or high-energy output applications, such as electrical cars. One potential solution is to design electrode materials with higher capacities and better performances.[1] Currently, graphite is a widely used anode material in the lithium ion battery, but the theoretical intercalation capacity of graphite is only 372 mAh/g.[2]

In the 1990s, it was discovered that the modified graphitic structure could lead to a higher capacity than the theoretical value of the perfect graphite.[3-7] Several hypothesises have been suggested to explain the enhanced capacities, but the mechanism remains unclear.[8, 9] Recently, enhanced lithium storage has been found in graphene, in which the graphene with disordered structure shows steep discharge-charge curves instead of the normal intercalation/de-intercalation plateau.[10-12] On the other hand, graphitic materials have been widely used in fabricating composite electrode materials for lithium ion batteries.[13-16] However, the capacity contribution of the graphitic materials, especially the disordered graphitic materials, is not well interpreted.[17, 18] In this study, disordered graphitic structures are produced using high-energy ball milling and their contribution to capacity and other lithium ion storage properties are investigated. By linking the disordered structure and the lithium ion storage properties, the mechanism of enhanced lithium storage is discussed.

Material and methods

Commercial graphite (CG) from Sigma Aldrich (particle size < 20 μm) was used as the starting material. Ball milling experiment was performed with a high-energy rolling ball mill with an external magnet to enhance the milling energy. [19] 4 g of graphite powders were milled with 4 hardened steel balls of 2.5 cm in diameter. The powder to ball weight ratio was 1:66. The rotating speed was 150 rpm and milling atmosphere was Ar gas at 300kPa.

The battery coin cells were assembled in an Ar filled glove-box. The anode was made by mixing the sample, carbon black and polyvinylidene fluoride (80:10:10 by weight ratio) in N-

methyl-2-pyrrolidone. The slurry was then coated on copper foils by 1*1 cm^2. The electrodes were dried in a vacuum oven for 24 h, weighed and moved into the glovebox. The electrodes used for multi-current charge-discharge test were pressed at 7 tons to increase the conductivity of the active material. A bulk electrode made for nuclear magnetic resonance (NMR) experiment was prepared using Teflon as binder. 90% active material and 10% Teflon were mixed with ethanol. The dispersion was heated at 70 °C with magnetic stirring, until forming slurry. The slurry was then transferred, dried and flatted to form free-standing electrode. The testing cells used a commercial consisting of 1M of $LiPF_6$ salt dissolved in a mixture of ethylene carbonate (EC), dimethyl carbonate (DMC) and diethyl carbonate (DEC) by 1:1:1 volume ratio and a polyethene separators. Lithium metal was used as a counter electrode.

The galvanic charge-discharge capacities were measured by a Land CT2001A system. The cyclic voltammetry (CV) and electrochemical impedance spectroscopy (EIS) were conducted with Ivium-n-Stat instrument. In both experiments, the cells were preconditioned by a 3-cycle charge and discharge before the test to avoid the influence of solid electrolyte interface formation. The CV tests were performed at 50 mV/s. Transmission electron microscopy (TEM) imaging was recorded using a JEOL-2100F FE-TEM microscope.

Solid-state NMR experiments were carried out on a BRUKER Avance3 NMR spectrometer, operating 194.2 MHz for ^{7}Li. Samples were packed into standard 4 mm magic angle spinning (MAS) rotors under Ar atmosphere, mounted in a BRUKER triple-resonance 4 mm MAS probe. MAS for CG was set to 7.5 kHz and to 13 kHz for the ball-milled carbon samples. A single 90 degree pulse with a nutation frequency of 100 kHz was used for lithium excitation. Recycle delays were set to 4 – 6 sec as determined beforehand. All ^{7}Li chemical shifts are given with respect to 1M LiCl solution.

Results and discussion

Fig. 1 shows the charge-discharge capacity of CG and ball-milled graphite samples at the current density of 0.1 C (37.2mA/g). The capacity increases with the milling time and all three milled samples have higher capacities than CG. However, in both charge and discharge curves of all milled samples, there is no intercalation or de-intercalation plateau Instead, the curves are steep indicating possible different charge/discharge mechanisms.[2]

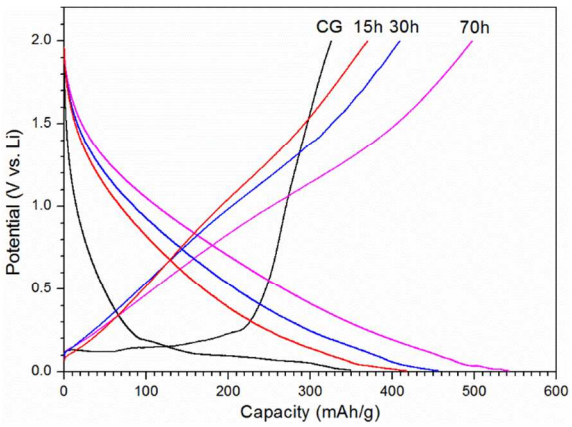

Fig. 1 Charge-discharge curves of CG and graphite milled in Ar for 15, 30 and 70 h.

The CV curves of various samples are shown in Fig. 2. For CG sample, there is a strong intercalation peak appearing below 0.17 V.[20] In the charging half-cycle, the corresponding de-intercalation peak appears at about 0.35 V. For the ball milled samples, the CV profiles change significantly. The sample milled for 15 h has a wider CV profile than CG. An extended milling leads to even wider CV profiles, which are similar to those of capacitors.[21, 22] The perfect physical capacitor should have shown a constant charge-discharge current at the experimental condition, so it implies that there might be chemical reactions at the same time, but the significant widening of CV profiles still indicates that there is a capacitive storage of lithium contributing to the lithium storage. The disappearance of the intercalation/de-intercalation peaks implies intercalation/de-intercalation is no longer the main mechanism contributing to the lithium storage.

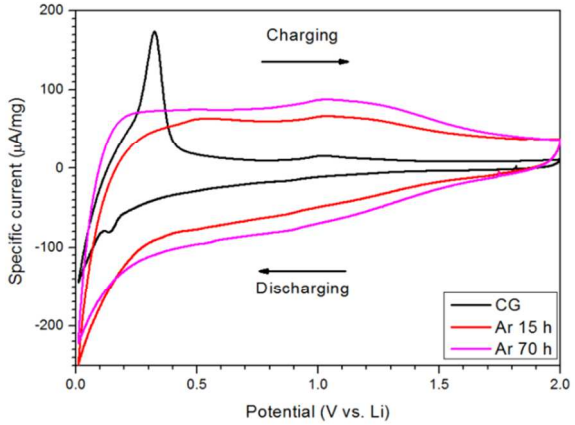

Fig. 2 CV curves of CG and graphite milled for 15 and 70 h in Ar gas.

Cyclability and multi-current charge-discharge experiments have been conducted to further investigate the battery performance of the milled samples. Fig. 3 shows the 0.1 C discharge capacity until 50 cycles. Three samples tested show similar stability during the test. The sample milled for 70 h shows the highest stable capacity of 316.6 mAh/g and retains 68% of its 3rd cycle capacity. CG shows a capacity of 225.7 mAh/g at 50th cycle and it is 64% of its 3rd cycle discharge capacity.

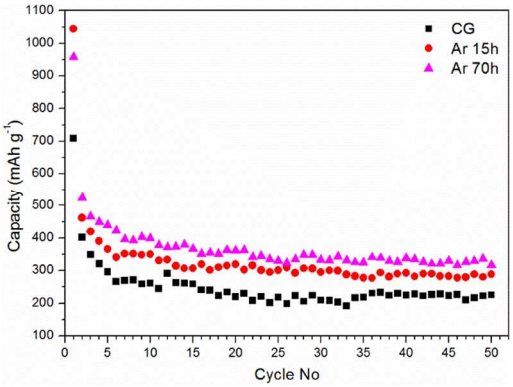

Fig. 3 Cyclability of CG and graphite milled for 15 and 70 h.

Samples milled for longer times show enhanced rate capacities than CG (Fig. 4). For example, Ar 70h sample has a capacity of 103 mAh/g at 1 C, which is 2.3 times higher than that of CG at the same current rate. The improvement should be due to the increased lithium capacity (more storage sites in ball milled graphite and easier access). In the case of CG, lithium ions need to diffuse a much longer distance. However, the capacities of all three samples drop down to about 20 mAh/g when the current rate increases to 5 C. Even though, the Ar 70h sample still shows better rate capacity behaviour than CG sample.

To understand storage mechanism in the milled samples, XRD was used to characterise crystallinity of all samples. XRD patterns of the milled samples show very broad (0 0 2) peaks at about 25° (Fig. 5). This is a sign of amorphisation of graphite.[23] TEM imaging also confirms the amorphous structure of the samples (Fig. 6). The starting material is polycrystalline graphite. After being milled for 15 h, the sample has begun to lose its graphitic structure (Fig. 6b). The sample contains mainly carbon clusters of the size down to about 10 nm after 70 h of ball milling (Fig. 6c).

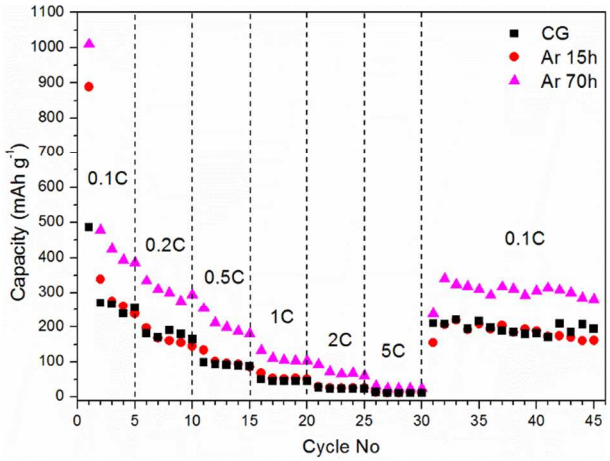

Fig. 4 Rate capacity of CG and graphite milled for 15 and 70 h.

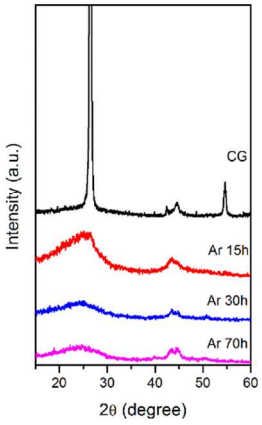

Fig. 5 XRD patterns of CG and milled graphite samples.

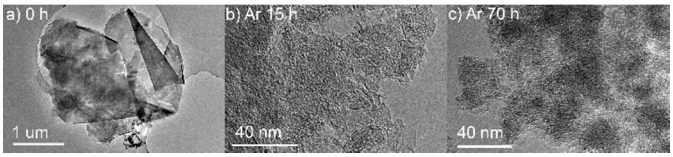

Fig. 6 TEM images of CG and ball milled samples.

Raman spectroscopy was also used to characterise disordering degree of the ball milled samples (Fig. 7). The Raman spectrum of CG contains four bands, labelled as D, G, D' and 2D band.[24, 25] For milled samples, only two bands can be seen from their Raman spectra, which are D and G bands. G and D' bands merge into one band and cannot be separated. 2D bands are very weak after 15 h ball milling and completely disappear for longer milling of 30 and 70 h. The intensity of the 2D band decreases with the increase of milling time, which is attributed to the disorder in c axis and the formation of turbostratic structures. Because of the weak bonding between the (002) basal planes, ball milling actions can easily destroy the original ordering between the basal planes and even cut large starting crystal down to very small sizes within the first period of milling stage. 2D band thus cannot be seen from the samples milled for 15 h or longer.[18] D and G bands are fitted to extract the information of the structure change. I_D/I_G is an indication of the structure defects in graphitic materials.[26] I_D/I_G is about 0.3 in CG, which indicates a good crystallinity and low level of defects (Fig. 8a). After ball milling, I_D/I_G rises up to 1.7 after 15 h of milling and then decreases during further milling. As reported previously,[20] this evolution of I_D/I_G is due to an equilibrium between disordering of graphitic structure induced by milling impact and the formation of ordered nanosized clusters. This is also confirmed by the evolution of FWHM of D bands (Fig. 8b). It increases from 45 to 110 cm^{-1} after 15 h ball milling and finally reaches 220 cm^{-1}. This widening also points to a distorted ring system.[26]

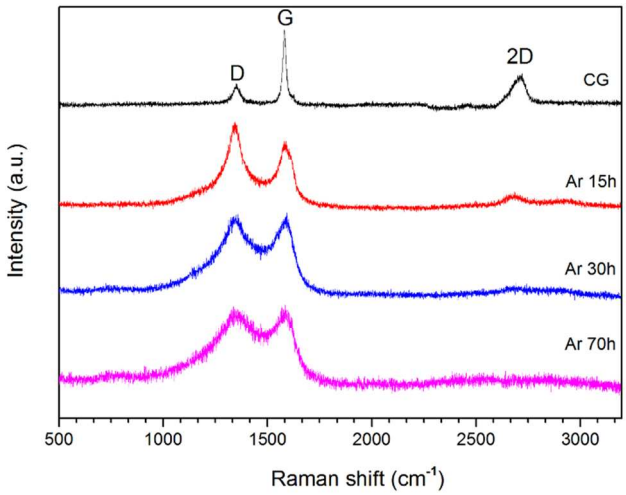

Fig. 7 Raman spectra of the ball-milled graphite samples.

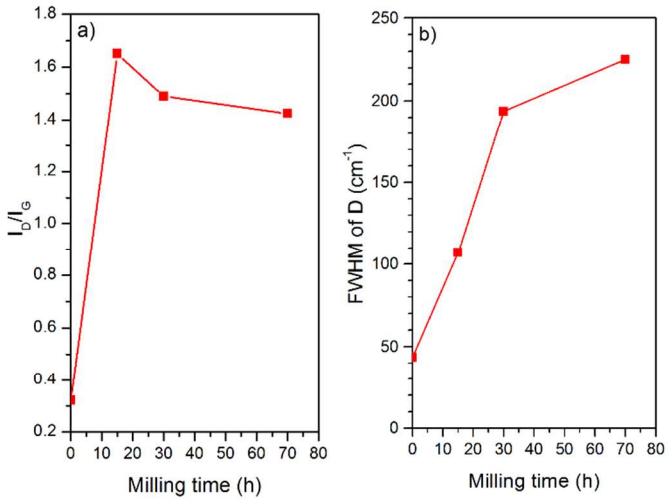

Fig. 8 Evolution of I_D/I_G (a) and the FWHM of the D bands (b) as function of milling time.

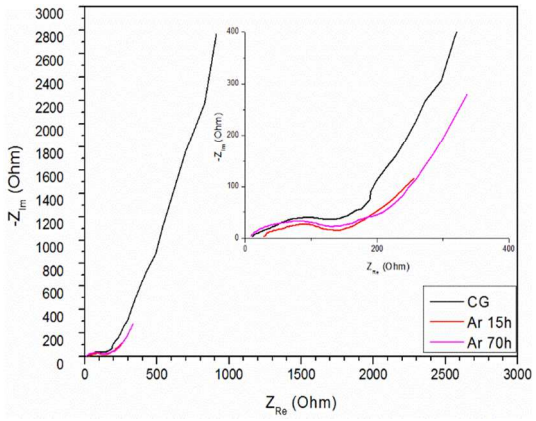

Fig. 9 Nyquist plot of CG and samples milled for 15 and 70 h.

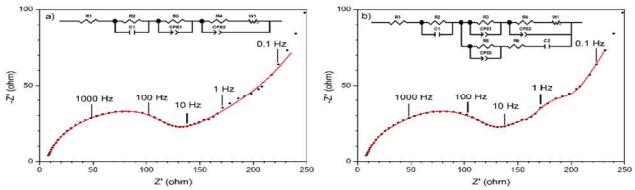

Fig. 10 Fitting of the EIS data by equivalent circuit method.

EIS result is shown in Fig. 9. CG has a typical Warburg impedance at low frequency whereas the milled samples do not have.[27] Ball milled samples have much lower resistance than CG in the mid to low frequency range. To understand the reason for this difference, the equivalent circuit has been used to fit the data. An example is shown in Fig. 10, which is the fitting of the Nyquist plot of Ar 70h with a two semi-circle model to describes the electrochemical property of the solid-state electrolyte interface (SEI) and sample surface (each is represented with a RC component and R represents resistor; CPE represents constant phase element).[27] The first RC component represents the impedance of lithium migration from solution to the solid electrolyte interface. The second semi-cycle represents the impedance of the lithium migration from SEI to graphite surface. The Warburg impedance (W1) represents the impedance of lithium diffusion into graphitic structure. R4 represents the resistance of the charge transfer between graphite and lithium atoms and CPE2 characterises the capacitance of graphite surface. When the circuit in Fig. 10a is the normally used circuit, another parallel circuit has been added to analogue the observed capacitor-like storage mechanism (Fig. 10b). In this parallel circuit, the first semi-cycle describes the SEI and the resistor (R6) analogues the resistance when the lithium migrates in the electrode material. The capacitor (C2) in this circuit is corresponding to the capacitive storage of lithium. The fitting in Fig. 10b is better than the one in Fig. 10a in mid frequency range. An interesting finding is that for CG, the capacitance of C2 is smaller than 10^{-5} F with the new fitting model. However, for the ball milled samples, it is higher than 10^{-2} F, which is 10^3 times larger than the one of CG. The equivalent circuit method is not always quantitatively accurate; however, such a large difference may be meaningful. It implies that there is a capacitor-like storage mechanism in samples milled in Ar. CV and charge-discharge experiments also support this hypothesis. This capacitor-like storage mechanism causes the increased capacity of samples milled in Ar.

^{7}Li solid state NMR clearly demonstrates the different lithiated carbon products formed in the graphitic samples with different disordering after being fully discharged (Fig. 11). Fig. 11a shows the ^{7}Li solid state NMR spectrum of CG after discharging. Three actual lithium signals are collected, which are enlarged in Fig. 11b. The peak with the largest area at about 43.6 ppm is corresponding to LiC_6, which is formed by the lithium intercalation into the interlayer of graphite.[28, 29] The peak at about 4.4 ppm is due to the defect related storage of lithium.[30] The sharp peak at about -1 ppm represents the lithium in the electrolyte.[30] After ball milling in Ar for 70 h, the lithium storage sites have been changed significantly (Fig. 11c and d). There are much more spinning sidebands in the 70h milled sample than that in CG, which means that the lithium is stored in a much more disordered and anisotropic environment.[31] Fig. 11d enlarges the only actual signal in this case, which is a broad peak at about 1 ppm. This is a strong evidence that, in this material, the mechanism of the lithium storage is defect-related storage.[28] Moreover, typical signals for the lithium intercalated graphite are not observed, confirming that lithium storage in this case is barely through intercalation mechanism and forming LiC_6, but through the storage at disordered structure.

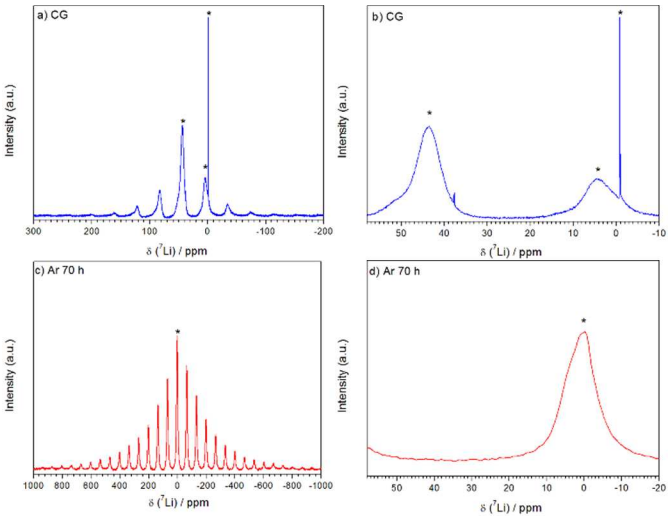

Fig. 11 ^{7}Li solid state NMR spectra of CG in a) and b); the spectra of Ar 70 h are shown in c) and d). 'Real' signals representing lithium in different chemical environments are labelled by '*' to distinguish from spinning sidebands. Multiple spinning frequencies are used to differentiate the actual signal and spinning sidebands.

Possible relationship between the disordered structure and the enhanced lithium storage is discussed in this section. The milling in Ar produces distorted rings which may increase the capacity via new storage mechanism. A dimensionless quantity *Dis* is defined to describe the distortion degree of the graphitic structure:

$$\mathrm{Dis} = \frac{\mathrm{ws}-\mathrm{wp}}{\mathrm{ws}} * \frac{\mathrm{A_D}}{\mathrm{A_G}} \quad (1)$$

ws: FWHM of D band of the sample;
wp: FWHM of D band of graphite that contains no distorted aromatic ring;
A_D: Area of D band of the sample;
A_G: Area of G band of the sample;

Wide D peak indicates more distorted graphitic ring system. Moreover, A_D/A_G should be considered since it indicates the quantity of the distorted rings.[20, 26]

At the same time, the intercalation and non-intercalation capacities are differentiated. By analysing the CV and galvanic discharge results, for CG the capacity below 0.2 V (vs. lithium metal) is intercalation capacity, and those above 0.2 V are contributed by non-intercalation process.[27, 32] For the samples milled in Ar, since neither intercalation-de-intercalation couple nor LiC_6 formation can be seen in CV and NMR spectra, respectively, and their capacities below 0.2 V are also very low, all the capacities are approximately taken as non-intercalation capacities. Afterwards, the excessive non-intercalation capacity of the sample is calculated:

$$C_e = C_s - C_g \quad (2)$$

C_e: excessive non-intercalation capacity of the sample;
C_s: non-intercalation capacity of the sample;
C_g: non-intercalation capacity of CG;

Excessive non-intercalation capacities of the milled samples are plotted against *Dis* (Fig. 12). A positive dependence can be seen between two quantities. It needs to be emphasised that since I_D/I_G decreases after 15 h of milling in Ar, there is no simple relationship between I_D/I_G and the excessive non-intercalation capacity. C_e is not correlated with the BET surface area (Fig S1). For example, the BET surface area of Ar 15h is the highest among the samples, but the Ar 15h sample shows much less C_e than the Ar 70h sample. It implies that the capacitor-like storage can mainly happen in the distorted graphitic structure, rather than simple surface absorption, edge sites or point-defect sites that can cause the increase of I_D/I_G but not the widening of the bands.[20, 24] The high surface area of ball milled graphite samples comes from a porous structure.[33] The pore size distribution change as the function of milling time is shown in Fig. S2. The pore size in the milled graphite samples in the range of 0.4-1.5nm and slightly increases with increasing milling time. The nanosized pore structure enhances the quasi-capacitive reaction and results in the increased capacitiy.

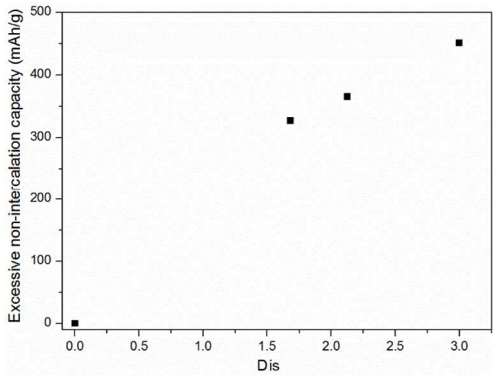

Fig. 12 The plot of excessive non-intercalation capacity against *Dis* of CG and ball milled samples.

Conclusions

The lithium storage mechanism in different graphitic structures has been studied systematically. The distorted graphitic structure has a higher capacity and new lithium storage mechanism that performs similarly to the electrochemical capacitor, which provides a greater capacity than the intercalation/de-intercalation storage. The capacitive capacity is positively dependent on the disordering of the graphitic structure and porous structure. In addition, the disordered graphitic structures exhibit better rate capacity than graphite.

Acknowledgements

The authors thank Miss Liting Hou from AT&M for her assistance with Raman spectroscopy analysis. The Australian Research Council is acknowledged for financial support under a Discovery Project and several LIEF grants for funding Deakin University's NMR, TEM and Raman facilities.

Notes and references

Electronic Supplementary Information (ESI) available: [BET surface area]. See DOI: 10.1039/b000000x/

1. R. Marom, S. F. Amalraj, N. Leifer, D. Jacob and D. Aurbach, *J. Mater. Chem.*, 2011, **21**, 9938-9954.

2. M. Yoshio, H. Wang, K. Fukuda, Y. Hara and Y. Adachi, *J. Electrochem. Soc.*, 2000, **147**, 1245-1250.
3. S. Sivakkumar, A. S. Milev and A. Pandolfo, *Electrochim. Acta*, 2011, **56**, 9700-9706.
4. F. Disma, L. Aymard, L. Dupont and J. M. Tarascon, *J. Electrochem. Soc.*, 1996, **143**, 3959-3972.
5. F. Salver-Disma, A. Du Pasquier, J.-M. Tarascon, J.-C. Lassègues and J.-N. Rouzaud, *J. Power Sources*, 1999, **81**, 291-295.
6. X.-L. Wu, Q. Liu, Y.-G. Guo and W.-G. Song, *Electrochemistry Communications*, 2009, **11**, 1468-1471.
7. X.-L. Wu , L.-L. Chen , S. Xin, Y.-X. Yin, Y.-G. Guo, Q.-S. Kong and Y.-Z. Xia, *ChemSusChem*, 2010, **3**, 703-707.
8. S.-H. Yeon, K.-N. Jung, S. Yoon, K.-H. Shin and C.-S. Jin, *J. Phys. Chem. Solids*, 2013.
9. T. Zheng, J. Reimers and J. Dahn, *Phys. Rev. B*, 1995, **51**, 734.
10. E. Yoo, J. Kim, E. Hosono, H.-s. Zhou, T. Kudo and I. Honma, *Nano Lett.*, 2008, **8**, 2277-2282.
11. P. Lian, X. Zhu, S. Liang, Z. Li, W. Yang and H. Wang, *Electrochim. Acta*, 2010, **55**, 3909-3914.
12. G. Wang, X. Shen, J. Yao and J. Park, *Carbon*, 2009, **47**, 2049-2053.
13. G. Wang, J.-H. Ahn, M. Lindsay, L. Sun, D. Bradhurst, S. Dou and H. Liu, *J. Power Sources*, 2001, **97**, 211-215.
14. J. Hassoun, G. Mulas, S. Panero and B. Scrosati, *Electrochem. Commun.*, 2007, **9**, 2075-2081.
15. Y. Zhang, X. Zhang, H. Zhang, Z. Zhao, F. Li, C. Liu and H. Cheng, *Electrochim. Acta*, 2006, **51**, 4994-5000.
16. T. Ramireddy, M. M. Rahman, T. Xing, Y. Chen and A. M. Glushenkov, *J. Mater. Chem. A*, 2014, **2**, 4282-4291.
17. M.-S. Balogun, M. Yu, C. Li, T. Zhai, Y. Liu, X. Lu and Y. Tong, *J. Mater. Chem. A*, 2014.
18. D. Lei, T. Yang, B. Qu, J. Ma, Q. Li, L. Chen and T. Wang, *Sustain. Energy*, 2014, **2**, 1-4.
19. Y. Chen, T. Halstead and J. Williams, *Mater. Sci. Eng., A*, 1996, **206**, 24-29.
20. S. Sivakkumar, J. Nerkar and A. Pandolfo, *Electrochim. Acta*, 2010, **55**, 3330-3335.
21. C. Largeot, C. Portet, J. Chmiola, P.-L. Taberna, Y. Gogotsi and P. Simon, *J. Am. Chem. Soc.*, 2008, **130**, 2730-2731.
22. M. Toupin, T. Brousse and D. Bélanger, *Chem. Mater.*, 2004, **16**, 3184-3190.
23. T. Xing, L. H. Li, L. Hou, X. Hu, S. Zhou, R. Peter, M. Petravic and Y. Chen, *Carbon*, 2013.
24. A. C. Ferrari, *Solid State Commun.*, 2007, **143**, 47-57.
25. S. Reich and C. Thomsen, *Philosophical Transactions of the Royal Society of London. Series A: Mathematical, Physical and Engineering Sciences*, 2004, **362**, 2271-2288.
26. A. Ferrari and J. Robertson, *Phys. Rev. B*, 2000, **61**, 14095.
27. D. Aurbach, B. Markovsky, I. Weissman, E. Levi and Y. Ein-Eli, *Electrochim. Acta*, 1999, **45**, 67-86.
28. K. Guérin, M. Ménétrier, A. Février-Bouvier, S. Flandrois, B. Simon and P. Biensan, *Solid State Ionics*, 2000, **127**, 187-198.
29. N. M. Trease, T. K. Köster and C. P. Grey, *Electrochem. Soc. Interface*, 2011, **20**, 69.
30. N. Takami, A. Satoh, M. Oguchi, H. Sasaki and T. Ohsaki, *J. Power Sources*, 1997, **68**, 283-286.
31. D. D. Laws, H.-M. L. Bitter and A. Jerschow, *Angew. Chem. Int. Ed.*, 2002, **41**, 3096-3129.
32. H. Wang and M. Yoshio, *J. Power Sources*, 2001, **93**, 123-129.
33. Y. Chen, J. Fitz Gerald, L. T. Chadderton and L. Chaffron, *Applied Physics Letters*, 1999, **74**, 2782-2784.